Magnetic circular dichroism and site-selective optically detected magnetic resonance of the deep amphoteric vanadium impurity in 6*H*-SiC

M. Kunzer, H. D. Müller, and U. Kaufmann
Fraunhofer-Institut für Angewandte Festkörperphysik, Tullastrasse 72, 79108 Freiburg, Germany
(Received 10 May 1993)

Magnetic-circular-dichroism (MCD) absorption and optically detected electron-spin-resonance (ESR) data for the neutral vanadium impurity, $V^{4+}(3d^1)$ on the α, β, and γ sites in 6*H*-SiC are presented and supplemented by linearly polarized absorption and luminescence spectra. An analysis of the linearly polarized spectra yields crystal-field-level schemes in zero magnetic field and an intensity parameter u for V^{4+} on each of the three Si sites. This information is used to account for the V^{4+} MCD zero-phonon-line positions, signs, and relative intensities without an adjustable parameter. Evidence of Jahn-Teller effects is found in both the V^{4+} ^2E ground and the $^2T_2$ excited states. The MCD-ESR technique, in the present case, is site selective. The V^{4+} resonances associated with the β and the γ site are virtually identical and cannot be distinguished by conventional ESR. The g factors for all three sites are satisfactorily explained within the framework of crystal-field theory.

I. INTRODUCTION

Silicon carbide, SiC, has attracted renewed interest as a semiconductor material for high-temperature, high-power, and high-frequency devices.[1,2] Compared with other compound semiconductors, the material development of SiC is still in an early stage. To improve the quality of both bulk substrates and epitaxial layers in particular, residual impurity and defect studies are required. A very often encountered impurity in Lely-type grown substrates is vanadium V. Its concentration can be in the high 10^{17} cm^{-3} range.

Near-infrared-absorption and luminescence studies of 6*H*-SiC crystals have revealed three sets of sharp zero-phonon lines (ZPL's) in the range 1.3–1.4 μm which, by comparison with corresponding ZPL's in 4*H*-SiC, were assigned to an impurity on the three different sites in 6*H*-SiC, the two quasicubic sites γ and β, and the trigonal α site. The electronic transitions in question were anticipated to be internal crystal-field transitions of $V^{4+}(3d^1)$, i.e., neutral V with respect to the Si^{4+} ion it replaces.[3–6] This assignment was supported by electron-spin-resonance (ESR) investigations. They revealed three distinct ESR signals which on the basis of the observed ^{51}V (nuclear spin $I=\frac{7}{2}$) hyperfine octet structures and the g-factor variations were assigned to $V^{4+}(3d^1)$ on the γ, β, and α sites, respectively.[3–5] Finally, photo-ESR studies of samples with different positions of the Fermi level gave very strong evidence that V_{Si} is an amphoteric impurity producing both a deep acceptor level, V^{4+}/V^{3+}, and a deep donor level, V^{4+}/V^{5+}, in 6*H*-SiC.

In this work, magnetic-circular-dichroism (MCD) results for the absorption ZPL's mentioned above are presented and explained in terms of $V^{4+}(3d^1)$ crystal-field-level schemes appropriate to the three specific sites. In addition, optically detected magnetic-resonance data are reported. They were obtained as microwave-induced changes in intensity of the sharp MCD absorption ZPL's. This MCD-ESR technique, in contrast to conventional ESR, is site selective and even can be made strain selective. The MCD-ESR data provide the first direct experimental link between the ZPL's in the 1.3–1.4-μm range and the ESR spectra of V^{4+} in 6*H*-SiC. With some modifications the MCD-ESR results confirm the previous assignments based on conventional absorption and ESR measurements.

II. EXPERIMENTAL DETAILS

The sample studied in this work is a Lely-type grown 6H polytype SiC platelet with a thickness of 0.5 mm. The hexagonal c axis is oriented perpendicular to the polished platelet planes. The sample geometry thus allows absorption and MCD absorption measurements only with the light beam along c. Luminescence measurements polarized $E\|c$ and $E\perp c$ were, however, possible. The sample is nominally undoped and is one of the compensated samples used in previous absorption, luminescence, and ESR studies. Such compensated samples reveal the 1.3–1.4-μm ZPL's already under dark equilibrium conditions.

A K-band (18–26 GHz) optically detected magnetic-resonance setup, built around a 4-T superconducting split-coil magnet, was used for MCD absorption and MCD-ESR studies. The MCD-ESR signals were obtained by monitoring the microwave-induced MCD intensity changes at a fixed photon energy. For the measurements reported here the optical beam and the external magnetic field H were parallel to the c axis of the sample. MCD-ESR measurements with a field direction a few degrees off c were performed to check the extremal positions of MCD-ESR lines for $H\|c$ but full angular rotation studies were not attempted.

III. RESULTS

Figure 1 in the upper part shows an MCD absorption spectrum as a function of photon energy. Only the ZPL's

0163-1829/93/48(15)/10846(9)/$06.00

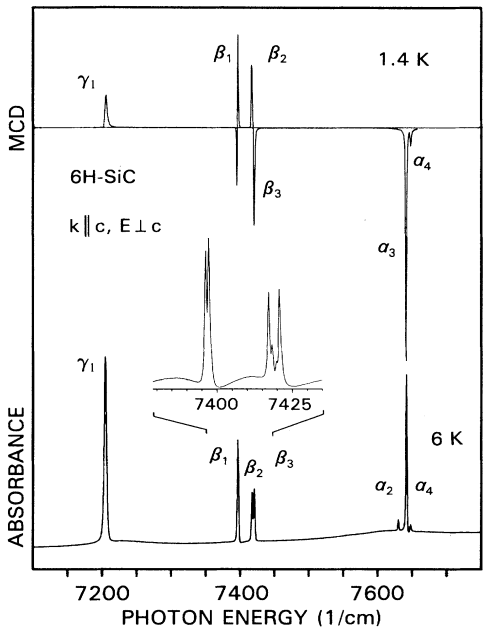

FIG. 1. MCD absorption ZPL's of $V^{4+}(3d^1)$ at $H=2.5$ T (upper spectrum). The lower trace, shown for comparison, is a conventional absorption spectrum. The blowup for the β site reveals that each β_i line consists of a doublet β_i', β_i''.

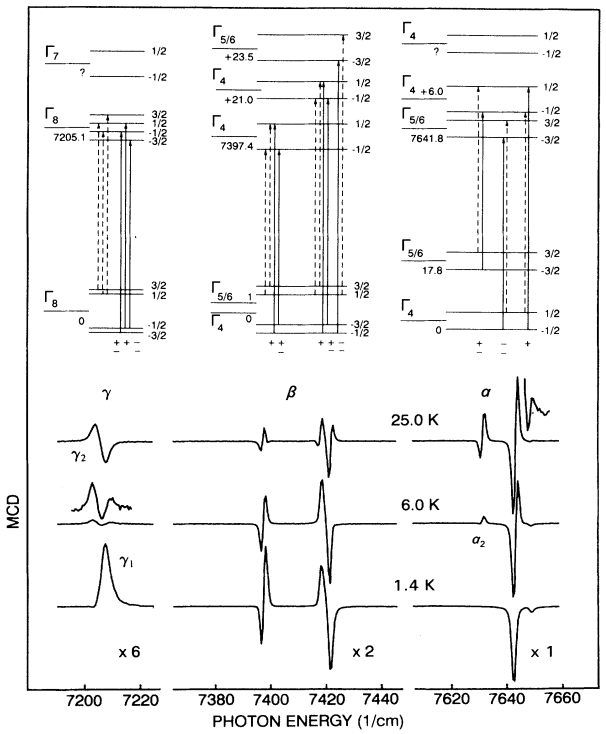

FIG. 2. Lower part: MCD spectra at three different temperatures recorded with better spectral resolution as in Fig. 1 ($H=2.5$ T). The 6- and the 25-K spectra are blown up in the ordinate direction by a factor of 2 and 2.4, respectively, compared with the 1.4-K trace. In addition, the γ and β lines are blown up compared to the α lines as indicated. Upper part: Zero-field crystal-field-level schemes for $V^{4+}(3d^1)$ on the three sites α, β, γ. Schematic Zeeman splittings are also indicated. See text for explanation of arrows and $\pm$ signs.

are shown but phonon replicas of course appear at higher energies. A very similar spectrum has been observed elsewhere.[7] For comparison, the conventional absorption spectrum of the same sample[3] is shown below. Each MCD structure is seen to have its conventional absorption counterpart. The intensities of the MCD signals are very strong, allowing good MCD spectra to be recorded at fields as low as 50 mT. At 1.4 K the relative intensities of the MCD lines are independent of magnetic-field strength with one exception. The negative part of the β_1 structure at least partially freezes out with increasing field strength. In addition the peak height of this negative signal decreases with decreasing spectral resolution. Significant changes in the MCD spectra occur when the temperature is raised. These are displayed in Fig. 2 for each site on an extended scale with a spectral resolution of ≈ 1 cm^{-1}. Perhaps the most interesting effect occurs for the γ site. At 6 K the γ_1 line acquires a derivative shape and a new line γ_2 appears 4.6 cm^{-1} below the zero of γ_1. Furthermore, this temperature increase reduces the MCD intensity of the γ site much stronger than that of the α or the β site. At 25 K the γ site MCD intensity is higher than at 6 K. The low temperature γ_1 line is replaced by a derivativelike structure γ_2 with opposite phase. For the β site the 1.4-K spectrum changes into three derivative structures at 25 K. Their zero positions agree in energy with the peak positions in conventional absorption to an accuracy of 0.5 cm^{-1}. For the α site a "hot" derivative structure α_2 appears in the 25-K spectrum which now also consists of three derivative structures. Again, their zeros agree in energy with the conventional absorption lines within 0.5 cm^{-1}. The level schemes above the MCD traces in Fig. 2 will be discussed in Sec. IV.

High-resolution (0.2 cm^{-1}) Fourier-transform infrared-absorption studies were performed for all three sets of ZPL's. No additional structure was observed for the γ and α lines but it was found that the half-width of the γ_1 line, 4 cm^{-1}, is larger than the widths of the β and α lines, 0.7 cm^{-1}. However, each of the three β lines, as shown in the inset of Fig. 1, consists of two components separated by 1.0 cm^{-1}. The same splitting was reported for the β_1 line by other workers for a different sample.[6] This indicates that an intrinsic splitting, not related to sample mounting induced strain and/or internal strains, is involved.

In Fig. 3 polarized luminescence spectra for the β and the α lines are shown. Special care was taken to suppress the influence of polarizing optical components in the optical path. Thus, the pronounced linear polarization effects observed with $E\|c$ and $E\perp c$ are due to the sample. Note that the 1-cm^{-1} splitting of the β_1 line is also visible in these luminescence spectra. At elevated temperatures (not shown) hot β lines corresponding to β_2 and β_3 in Fig. 1 appear in the luminescence spectra.

MCD-ESR spectra recorded with low optical resolu-

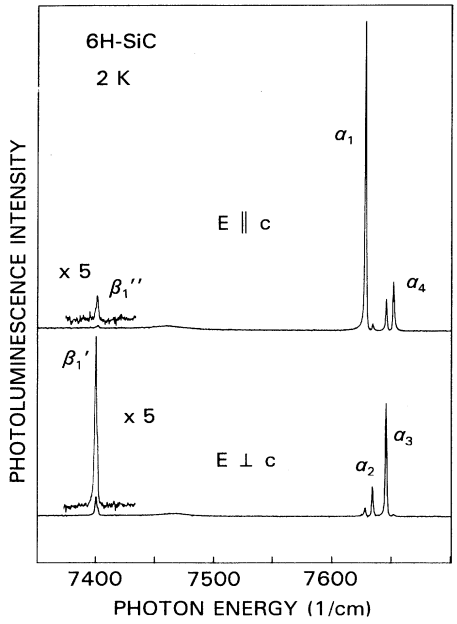

FIG. 3. Linearly polarized luminescence spectra of V^{4+} for the β and the α sites excited with the uv lines of a Kr-ion laser.

tion (≈ 4 cm^{-1}) on the peaks of the γ, β, and α lines, respectively, are shown in the overview of Fig. 4. The best resolved signal is the hyperfine octet detected on the α lines. It is characterized by $g_{\parallel}=1.749$ and $A_{\parallel}=93$ G in full agreement with the ESR values determined previously at 5 K. In addition to the allowed lines, weak lines due to forbidden transitions ($\Delta m_I=\pm 1$) are seen. The corresponding spectra for the γ and β sites occur at larger g values and are similar to each other although the hyperfine structure is better resolved for the β site.

The β-site spectrum consists of two overlapping octets having individual linewidths between 2 and 3 mT. This could be proved by monitoring the spectrum with better spectral resolution (≈ 1 cm^{-1}) on the peak and on the high-energy wing of the negative β_3 line in Fig. 1, respectively, see Fig. 5. Again, weaker forbidden lines are seen, particularly in the lower-field region. The lower-field octet is more clearly seen when detected on the β_3 peak while the higher-field octet is well visible when detected on the wing. In addition, it is seen that these MCD-ESR measurement conditions slightly affect the position of the resonance lines. This effect is most pronounced for the uppermost β higher-field octet line in Fig. 5 but it is also visible for the lowest lower-field octet line and this has consequences for the g factors of the two octets. These two g factors for the β site, evaluated under three measurement conditions are listed in Table I. Those evaluated under low optical resolution are seen to be very close to the g factors inferred from conventional ESR for V^{4+} on the β *and* the γ sites, respectively. The γ-site resonance in Fig. 4 also reveals an indication of a line near 0.81 T suggesting that the spectrum in this case too consists of two overlapping octets with somewhat broader individual lines. The g factors for these two octets obtained from the spectrum in Fig. 4 are virtually identical with those of the β site, compare Table I.

IV. DISCUSSION AND CONCLUSIONS

The ZPL's of a given group of lines in Figs. 1 and 2 do not overlap with vibronic sidebands of any significant intensity from another group of lines. Thus, the MCD-ESR technique not only establishes that the same defect is responsible for the optical spectra in Figs. 1 and 2 and for the resonance spectra in Figs. 4 and 5. In the present case the technique is also site selective, which means that,

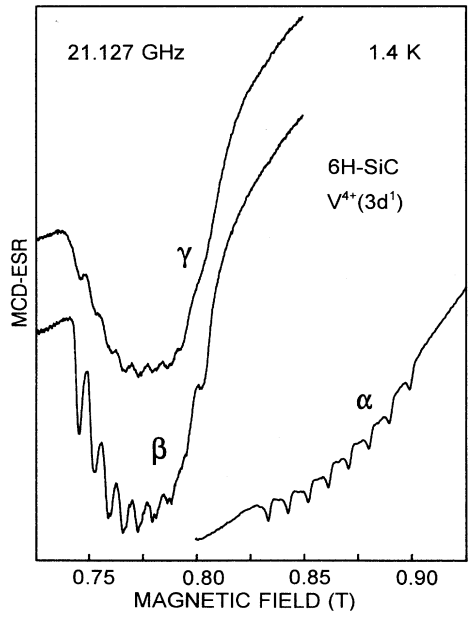

FIG. 4. MCD-ESR spectra detected with low optical resolution on the γ_1, β_3, and the α_3 lines in Fig. 1, respectively.

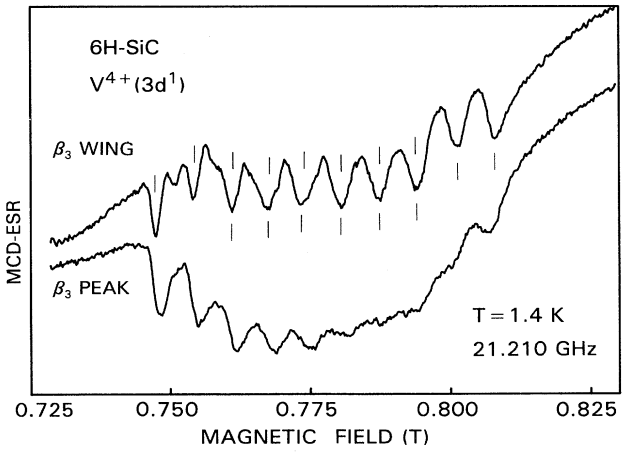

FIG. 5. MCD-ESR spectra detected with high optical resolution on the peak and on the high-energy wing of the β_3 ZPL, respectively.

TABLE I. Measured ground-state g factors of V^{4+} in 6H-SiC. hr denotes high resolution and lr denotes low resolution.

Site	Technique	$g_{\parallel}(\Gamma_{5/6})$	$g_{\parallel}(\Gamma_4)$	$g_{av}\equiv g_1$
α	Zeeman[a]/MCD-ESR	2.0[a]	1.749	1.875
β	MCD-ESR (hr wing)	1.972	1.936	1.954
	MCD-ESR (hr peak)	1.970	1.939	1.954
	MCD-ESR (lr peak)	1.969	1.941	1.955
	ESR[b]	1.967	1.946	1.956
γ	MCD-ESR (lr peak)	1.968	1.941	1.955

[a]Reference 13.
[b]Reference 4.

e.g., on the α lines only the resonance spectra of defects on the α site can be observed. The site correlation between the absorption ZPL's and the ground-state ESR spectra suggested previously is herewith established although with modifications.

In the following sections the ground-state resonance data and the MCD absorption spectra will be discussed in the frame of crystal-field theory. It will be shown that most of the data are fairly well explained if the theory is applied to the simplest case among the 3d transition metal ions, namely the electron configuration $3d^1$ which is that of a V^{4+} ion.

A. Crystal-field theory for $V^{4+}(3d^1)$

A tetrahedral crystal field lifts the fivefold d-orbital degeneracy of the ^2D free-ion V^{4+} ground state such that an E orbital doublet lies below the orbital triplet T_2; see Fig. 6.[8] The splitting energy denoted by $10Dq$, from a comparison with GaP:V^{4+},[9] is expected to be near 7000 cm^{-1} or somewhat larger. In the absence of fields of lower than cubic symmetry but with spin-orbit coupling included, the ^2E ground state becomes a Γ_8 quartet state while the excited $^2T_2$ state is split into a lower Γ_8 quartet and a Γ_7 doublet higher in energy by $\frac{3}{2}\lambda$. Here, the parameter λ is the spin-orbit coupling constant. For the V^{4+} free ion, $\lambda_0=248$ cm^{-1}. If the crystal field contains, compared with $10Dq$, a small trigonal component as is the case for all three sites in 6H-SiC, the Γ_8 ^2E ground state is split into two Kramers doublets transforming as Γ_4 and $\Gamma_{5/6}$ in C_{3v} symmetry. The $^2T_2$ state splits into three Kramers doublets, two transforming as Γ_4 and one as $\Gamma_{5/6}$. The splittings between these three Kramers levels depend on the relative magnitude and sign of λ and the trigonal field parameter $\Delta\equiv 3K$ and usually must be extracted from experimental data. There is a simple second-order relation[10] connecting the ^2E splitting δ to the spin-orbit (λ') and trigonal field (K') matrix elements between ^2E and $^2T_2$

$$\delta=\frac{4K'\lambda'}{10Dq} . \tag{1}$$

If K' is defined as in Ref. 10, Γ_4 is below the $\Gamma_{5/6}$ level for $K'>0$. An evaluation of the absorption spectra in Fig. 1 gives $\delta(\beta)=1.0$ cm^{-1} and $\delta(\alpha)=17.8$ cm^{-1} for the ^2E splitting of the β and α sites, respectively. The C_{3v} symmetry labeling of the Kramers doublets in Fig. 6 can be inferred by comparing the electric dipole selection rules in Fig. 6 for the optical transitions shown with the observed polarization behavior for linearly polarized light. The labeling in the schematic scheme of Fig. 6 is appropriate for V^{4+} on the α site. Compared with the scheme previously suggested for this site,[4,5] the Γ_4 and $\Gamma_{5/6}$ ground-state levels as well as the lowest Γ_4 and $\Gamma_{5/6}$ levels within $^2T_2$ are interchanged. Both schemes account fairly well for the observed polarization behavior in luminescence but the present one is dictated by the absorption spectra under $E\perp c$. For instance, the observation of line α_4 and the nonobservation of α_1 in Figs. 1 and 2 is in line with the present scheme but not with the previous one.

In order to understand the different signs of the MCD lines in Figs. 1 and 2 one needs zero-field-level schemes of V^{4+} for *each* site as shown in the upper part of Fig. 2. They are based on the predictions of crystal-field theory as discussed above and on the linear polarization behavior of the ZPL's in conventional absorption, Fig. 1, and luminescence, Fig. 3. Linear polarization effects and relative intensities are treated in detail in Sec. IV D. Since trigonal field splittings for the γ site vanish within the width of the ZPL perfect cubic symmetry is assumed

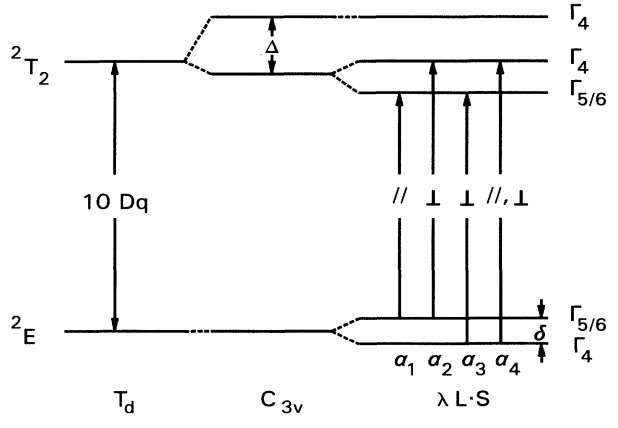

FIG. 6. Crystal-field-level scheme of a $3d^1$ ion in trigonally distorted tetrahedral symmetry. The arrows correspond to $E1$ allowed transitions. Their polarization characteristics $E\|c$ or $E\perp c$ are indicated. The symmetry assignments of the levels and their ordering correspond to V^{4+} on the α site.

in the γ scheme in Fig. 2. Note that for the β scheme in Fig. 2 the ordering of the two highest Kramers levels Γ_4 and $\Gamma_{5/6}$ is opposite to that expected from first-order crystal-field theory. The small overall splitting within $^2T_2$ is a clear indication that the first-order spin-orbit interaction is quenched by a dynamic Jahn-Teller effect.[11] In such a case second-order spin-orbit and/or trigonal field corrections can push the $\Gamma_{5/6}$ level above both Γ_4 levels. The MCD spectra will be discussed in Sec. IV E.

B. Ground-state g factors

The g factors for $H\|c$ of the two ground-state doublets, to the order $K'/10Dq$ and $\lambda'/10Dq$, are given by[10]

$$g_\parallel(\Gamma_4)=2[1+2k'(-2K'-\lambda')/10Dq]\ , \tag{2a}$$

$$g_\parallel(\Gamma_{5/6})=2[1+2k'(2K'-\lambda')/10Dq]\ . \tag{2b}$$

Here, k' is a covalency reduction factor appropriate to matrix elements of the orbital angular-momentum operator $\mathbf{L}$ between the E and the T_2 states. Note that if K' tends to zero, i.e., cubic symmetry, both $g_\parallel$ factors approach the crystal-field value of g_1 which is the g factor describing the isotropic part of the Zeeman interaction within the cubic $\Gamma_8\ ^2E$ state[12]

$$g_1=2-4k'\lambda'/10Dq\ . \tag{3}$$

Using the approximate relation $\lambda'\approx k'\lambda_0$, a typical value of k', $k'\approx 0.9$, $\delta(\alpha)=17.8\ \mathrm{cm}^{-1}$, and $10Dq\approx 7600\ \mathrm{cm}^{-1}$ from Fig. 1, one obtains from Eq. (1) for V^{4+} on the α site, $K'\approx 247\ \mathrm{cm}^{-1}$. The $g_\parallel$ values predicted by Eqs. 2(a) and 2(b) are then given by $g_\parallel(\Gamma_4)=1.75$ and $g_\parallel(\Gamma_{5/6})=2.03$ in excellent agreement with the values determined by ESR and MCD-ESR for Γ_4 and by Zeeman studies[13] for $\Gamma_{5/6}$, respectively.

Using $\delta(\beta)=1.0\ \mathrm{cm}^{-1}$, $10Dq\approx 7400\ \mathrm{cm}^{-1}$, and the same value of λ' as above, one obtains from Eq. (1) for the β site, $K'\approx 8\ \mathrm{cm}^{-1}$. With these values the average g factor g_{av} of the ^2E ground-state levels, $g_{\mathrm{av}}=\frac{1}{2}[g_\parallel(\Gamma_{5/6})+g_\parallel(\Gamma_4)]\equiv g_1$, according to Eq. (3) is predicted to be ≈ 1.90, i.e., smaller than the experimental value of 1.95. This deviation neither results from the neglect of higher-order crystal-field terms $(\lambda'/10Dq)^2$ in Eqs. (2) and (3) nor can it be accounted for by Jahn-Teller effects.[12,14] For $H\|c$ in 6H-SiC, which corresponds to $H\|\langle 111\rangle$ in zinc blende, first-order Jahn-Teller effects on the g factors are not expected. It is therefore suggested that the neglect of configuration mixing and/or ligand contributions to the g factors cause this slight discrepancy. It is noted that the same problem is encountered for the ^2E ground-state g factor of V^{4+} in GaP.[15] The g-factor difference

$$\Delta g_\parallel=g_\parallel(\Gamma_{5/6})-g_\parallel(\Gamma_4)=16k'K'/10Dq \tag{4}$$

is predicted as 0.016 which is smaller than measured. This may be an indication of a dynamic Jahn-Teller effect which quenches the ^2E trigonal field splitting by the Ham reduction factor p.[12] The true crystal-field value of K' for the β site may therefore be larger than the value derived above thus giving an increased $\Delta g_\parallel$ value.

The value of $\Delta g_\parallel(\gamma)$ for the γ site equals $\Delta g_\parallel(\beta)$; see Table I. According to Eqs. (1) and (4) this indicates that $\delta(\gamma)\approx\delta(\beta)$. Thus, the ^2E trigonal field splitting of V on the γ site must be similar to the resolved 1.0-cm^{-1} splitting of the β site. On the other hand, the increased line broadening in the γ-site MCD-ESR spectrum indicates that the effects of internal random strains are more pronounced for the γ than for the β site. This is also observed in the optical spectra where the γ site mimics a truly cubic site behavior; see also Sec. IV E. Since the site-selective MCD-ESR technique gives virtually identical spectra for the γ and the β sites, the site assignment suggested previously in the 9.5-GHz ESR spectrum[4,5] requires some modification. It is proposed that the two hyperfine octets observed by ESR near $g=1.95$ result from the different g factors of the $\Gamma_{5/6}$ and the Γ_4 level of one site, the γ and β sites giving indistinguishable contributions to both octets. In other words, ESR at 9.5 GHz does not discriminate between the β and the γ sites.

C. Strain effects in MCD-ESR

The resonance properties of a cubic ^2E state are known to be very sensitive to internal strains.[12] This is also the case when a weak trigonal field splits the ^2E, as long as the trigonal splitting does not substantially exceed typical splittings ($1\ \mathrm{cm}^{-1}$) induced by internal strains. Such a situation is encountered here for the γ and β sites.

When the β_3 MCD line is monitored in its high-energy wing, one selects β sites which experience large internal strains since they are the major source for the broadening of the optical ZPL's. The increased transition energy at the high-energy wing as compared to the peak results at least in part from a trigonal strain-induced increase in the ^2E trigonal field splitting δ. According to Eq. (1) this transforms into a strain-enhanced K' value. From Eqs. 2(a) and 2(b) it is now seen that this effect leads to a strain-enhanced $g_\parallel(\Gamma_{5/6})$ and a strain-reduced $g_\parallel(\Gamma_4)$ value, i.e., an increase in the g-factor difference. In other words, the $\Gamma_{5/6}$ lower-field octet is expected to move to lower fields while the Γ_4 higher-field octet should move to higher fields when the MCD-ESR is monitored on the β_3 high-energy wing as compared to the peak. Equations (2a) and (2b) also show that, for the given parameter set $K'\approx 8\ \mathrm{cm}^{-1}$, $\lambda'\approx 223\ \mathrm{cm}^{-1}$, the relative strain effect is larger for the Γ_4 higher-field octet than for the $\Gamma_{5/6}$ lower-field octet. All these predictions are confirmed by the β-site MCD-ESR spectra in Figs. 4 and 5. In particular it should be noted that the field equivalent of the octets's g-factor difference amounts to about one hyperfine spacing in the β peak spectrum of Fig. 4 and to about two such spacings in the wing spectrum of Fig. 5.

D. Relative intensities in zero field under linear polarization

The linearly polarized absorption spectra in the lower part of Fig. 1 and the luminescence spectra in Fig. 3 not only definitely establish the zero-field-level schemes in the top of Fig. 2 and in Fig. 6, they also help to elucidate the signs and intensities of the MCD absorption lines.

It is a completely general result based on group theory that the relative transition probabilities, (RTP's) of all six optical transitions in C_{3v} symmetry that can originate from a $\Gamma_8^{(1)} \rightarrow \Gamma_7$ and a $\Gamma_8^{(1)} \rightarrow \Gamma_8^{(2)}$ transition in cubic symmetry can be described by two independent parameters.[16] In the present case where the orbital parts of all five C_{3v} states in question derive from d orbitals, compare Fig. 6, there must be a simple relation between thee two parameters. We find for the parameters D_0' and D' defined in Ref. 16 that $D_0'^2 = 2D'^2$ with both D_0' and D' being real here. Thus, the RTP's for all six possible transitions can be expressed by a single real parameter u, $0 \leq u \leq 1$ as defined in Ref. 16. However, the RTP's quoted in Table XIV of Ref. 16 cannot be compared directly with our data because the total intensity normalization condition used there is not appropriate in the present case. Here, we must require that the total $^2E \rightarrow {}^2T_2$ intensity is a constant independent of the strength of the trigonal perturbation. The $E \| c$ and $E \perp c$ RTP's listed in Table II in terms of the parameter u have been derived with the help of Table XIV in Ref. 16 under the above normalization condition.

It should be noted that $u = 1$ corresponds to the case of cubic symmetry and that u values close to 1 and 0 represent weak and strong trigonal fields, respectively. It will be seen below that $u(\alpha) = 0.08$, $u(\beta) = 0.85$, and $u(\gamma) \approx u(\beta)$ give pretty good overall agreement between predicted and measured relative intensities.

The total, relative $E \perp c$ intensity of each site at 6 K can be obtained from Table II by summing up the RTP's of those transitions which give a significant contribution to the ZPL's at this temperature. Using the u values quoted above for the three sites, the total relative intensities are 0.49, 1, and 0.58 for the α, β, and the γ sites, respectively. The corresponding measured intensities from the absorption spectrum in Fig. 1 are 0.45, 1, and 2.4. Assuming that the impurity has no site preference, agreement within a factor of ≈ 4 is thus obtained.

Table II is divided into four blocks corresponding to absorption (a) and emission (e) data for the α and β lines. The experimental intensities in columns 5,6 within each block are normalized such that the strongest line has unity intensity. The calculated intensities in columns 7,8 are obtained from the RTP's in columns 3,4 with appropriate Boltzmann factors and are normalized accordingly. With $u(\beta) \approx 0.85$ and $u(\alpha) \approx 0.08$, agreement usually better than within a factor of ≈ 3 is obtained. The only significant deviation occurs for the hot α_2 absorption line. This is very likely due to the fact that the true electron temperature of the sample is higher than the nominal temperature quoted in Fig. 1. The otherwise good agreement gives us confidence in the line assignments. There are, however, two cases where the predicted intensities are zero whereas those observed are significant. This concerns the β_3' absorption line under $E \perp c$ and the α_3 emission line under $E \| c$. Misorientation effects can be excluded for α_3. Thus, the α_3 parallel intensity most likely results from a mixing of the lower Γ_4 level with the nearby $\Gamma_{5/6}$ level within $^2T_2$ in Fig. 6, induced by internal tetragonal strains. This has consequences for the sign of

TABLE II. Line assignments and relative intensities under $E \| c$ and $E \perp c$ for the sites β and α in zero-field absorption (a) and emission (e).

ZPL	Transition in C_{3v}	RTP		Experimental intensities		Calculated intensities	
		$\|\|$	$\perp$	$\|\|$	$\perp$	$\|\|$	$\perp$
(a)							
β_1'	$\Gamma_{5/6} \rightarrow \Gamma_4$	0	$\frac{1}{2}-\frac{3}{8}u$		0.88	0	0.85
β_1''	$\Gamma_4 \rightarrow \Gamma_4$	$\frac{1}{2}-\frac{1}{2}u$	$\frac{1}{4}u$		1	0.35	1
β_2'	$\Gamma_{5/6} \rightarrow \Gamma_4$	0	$\frac{3}{8}u$		0.59	0	1.50
β_2''	$\Gamma_4 \rightarrow \Gamma_4$	$\frac{1}{2}u$	$\frac{1}{8}u$		0.23	2.00	0.50
β_3'	$\Gamma_{5/6} \rightarrow \Gamma_{5/6}$	$\frac{1}{2}$	0		0.14	2.35	0
β_3''	$\Gamma_4 \rightarrow \Gamma_{5/6}$	0	$\frac{1}{2}-\frac{3}{8}u$		0.62	0	0.85
(e)							
β_1'	$\Gamma_4 \rightarrow \Gamma_{5/6}$	0	$\frac{1}{2}-\frac{3}{8}u$	0.05	1	0	1
β_1''	$\Gamma_4 \rightarrow \Gamma_4$	$\frac{1}{2}-\frac{1}{2}u$	$\frac{1}{4}u$	0.15	0.43	0.41	1.18
(a)							
α_2, hot	$\Gamma_{5/6} \rightarrow \Gamma_4$	0	$\frac{1}{2}-\frac{3}{8}u$		0.07	0	0.01[a]
α_3	$\Gamma_4 \rightarrow \Gamma_{5/6}$	0	$\frac{1}{2}-\frac{3}{8}u$		1	0	1
α_4	$\Gamma_4 \rightarrow \Gamma_4$	$\frac{1}{2}-\frac{1}{2}u$	$\frac{1}{4}u$		0.06	0.98	0.04
(e)							
α_1	$\Gamma_{5/6} \rightarrow \Gamma_{5/6}$	$\frac{1}{2}$	0	1	0.02	1	0
α_2, hot	$\Gamma_4 \rightarrow \Gamma_{5/6}$	0	$\frac{1}{2}-\frac{3}{8}u$	0.02	0.09	0	0.12[b]
α_3	$\Gamma_{5/6} \rightarrow \Gamma_4$	0	$\frac{1}{2}-\frac{3}{8}u$	0.11	0.38	0	0.94
α_4, hot	$\Gamma_4 \rightarrow \Gamma_4$	$\frac{1}{2}-\frac{1}{2}u$	$\frac{1}{4}u$	0.16	<0.01	0.12[b]	<0.01[b]

[a]Includes Boltzmann factor for the nominal temperature of 6 K quoted in Fig. 1.

[b]Includes Boltzmann factor calculated with an electron temperature of 4.2 K instead of the nominal bath temperature quoted in Fig. 3.

the α_4 MCD absorption line. Finally, we can understand why for the α site the highest-energy absorption transition $\Gamma_4 \rightarrow \Gamma_4$ in Fig. 6 was not observed. Its $E \perp c$ intensity is a factor of 2 less than the α_4 intensity thus being probably too weak to be detectable.

It is finally mentioned that additional V^{4+} α, β, and γ luminescence lines labeled *V-X*, not observed here, have been reported elsewhere[13] for a "6*H*"-SiC sample. Almost certainly this sample is not a pure 6*H* polytype and the additional lines also arise from isolated V^{4+} on Si sites but situated in stacking faulted regions of the crystal where they experience slightly different crystal fields.

E. MCD absorption

The MCD absorption signal $S(h\nu)$ as a function of photon energy $h\nu$ is defined as the difference in absorption between left (σ_+) and right (σ_-) circularly polarized light when the sample is placed in an external magnetic field H and the light propagates along the field direction. Thus, $S(h\nu)$ is proportional to $\alpha_+(h\nu)-\alpha_-(h\nu)$ where α_+ and α_- are absorption coefficients for σ_+ and σ_- polarized light, respectively. $S(h\nu)$ may acquire either sign depending on the relative magnitude of α_+ and α_- at a given photon energy. For instance, a spectrally "free-standing" transition between a ground- and an excited-state Zeeman level gives a positive (negative) MCD line if the transition in question is σ_+ (σ_-), polarized.

When a magnetic field is applied along c the Γ_8 states and the Kramers doublets in Fig. 2 split into time-conjugated Zeeman levels labeled as $\pm\frac{1}{2}$ or $\pm\frac{3}{2}$ according to their symmetry properties. The electric dipole ($E1$) operators for left ($x+iy$) and right ($x-iy$) circularly polarized light can induce σ_+ and σ_- optical transitions between these levels. The usual $E1$ allowed $\Delta m_j = 1$ (σ_+) and $\Delta m_j = -1$ (σ_-) transitions are shown in Fig. 2. Those starting from the lowest (α) or the two lowest (β,γ) Zeeman levels are shown as full arrows ordered for each site from the left to the right in the sequence of increasing zero-field energy. Their time-conjugated transitions[17] starting from the corresponding upper Zeeman levels are shown as dashed arrows. The latter transitions have exactly the same transition probabilities as the original ones but the opposite circular polarization. At $T=1.4$ K, $H=2.5$ T, and $g\approx 2$ they are almost frozen out since the population ratio of the lowest Zeeman level and its corresponding excited level is about 10:1. Thus, at 1.4 K one expects to observe essentially transitions corresponding to the full arrows in Fig. 2 with the following exception: In the present case, i.e., $H \| c$ which corresponds to $H \| \langle 111 \rangle$ in zinc blende also, $\Delta m_j = \pm 2$ transitions are $E1$ allowed by symmetry and cannot be neglected. The reason is the third-order S_i^3 term in the linear Zeeman interaction which mixes the $\pm\frac{3}{2}$ levels. These $\Delta m_j = \pm 2$ transitions are not shown in Fig. 2, simply not to overload the figure, but their presence is indicated by the $\pm$ signs below the solid arrows. The upper $\pm$ signs give the $\sigma_\pm$ polarization characteristics of the $|\Delta m_j| = 1$ transitions while the lower signs correspond to $\sigma_\pm$ of the $|\Delta m_j| = 2$ transitions. In the subsequent analysis the latter are taken into account.

For a comparison of the MCD ZPL signs and intensities with theory one requires relative $\sigma_\pm$ transition probabilities for the transitions in question. These were derived[18] in full generality and are complicated looking expressions depending on four parameters. Two of them, in the present case, are simple numbers. From their definition in Eq. (35) of Ref. 18 we find $\gamma = -1/\sqrt{2}$ for the $\Gamma_8\ ^2E$ state and $\gamma' = (\sqrt{2}/2)(5-3\sqrt{3})$ for the $\Gamma_8\ ^2T_2$ state. A further simplification results from the observation that the relative signs and intensities of the MCD ZPL's are practically field independent (except the negative part of β_1). Thus, a situation where all Zeeman splittings are much smaller than the widths of the ZPL's can be exploited. This means that RTP's from different transitions contributing to a specific ZPL can simply be summed up. These RTP's were derived with the help of Table XIV in Ref. 18 again using the normalization condition that the total $^2E \rightarrow {}^2T_2$ intensity is independent of the strength of the trigonal field as in Sec. IV D. They are listed in column 3 of Table III. The nice result is that they depend on a single parameter which turns out to be the u parameter derived in the previous section for the three sites. We can therefore account for the 1.4-K MCD ZPL signs and relative intensities without any free parameter.

The relative, calculated MCD intensities at 1.4 K of the six MCD lines in Fig. 1 are listed in column 4 of Table III. They were obtained from column 3 with the appropriate u parameters for the three sites neglecting the weak contributions from the time-conjugated transitions and with nonunity Boltzmann factors where indicated. It should be noted first that the predicted MCD line signs, except for line α_4, agree with the observed signs, as compared with column 5 of Table III. Second, for these five ZPL's also the relative intensities observed agree with those calculated within a factor of ≈ 2. However, the wrong MCD sign is predicted for the weak α_4 line. This is not totally unexpected since evidence has been presented in Sec. IV D that the excited Γ_4 level involved in the transition is mixed with the nearby $\Gamma_{5/6}$ level by internal tetragonal strains. This means that the α_4 transition "borrows" *negative* MCD intensity from the strong α_3 transition. An admixture of only 8% is sufficient to obtain a negative α_4 MCD intensity. The incomplete freeze-out of the negative part of the β_1 MCD line at 1.4 K is not fully understood. It is probably related to the 1-cm^{-1} ground-state splitting of V^{4+} on the β site in zero field.

The increased complexity of the MCD spectra at temperatures above 1.4 K in Fig. 2 results from the increased population of the higher-lying ground-state Zeeman levels. As a consequence the dashed, time-conjugated transitions in the level schemes of Fig. 2 gain in intensity as compared to the original solid transitions. Since the two types of transitions have opposite circular polarization and since they are spectrally separated by Zeeman splittings, each positive or negative MCD line at 1.4 K is expected to evolve into a derivativelike structure at elevated

temperatures. This is clearly the case for all α and β lines in Fig. 2. The γ-site spectra, however, reveal unexpected features. If the γ site has perfect cubic symmetry as assumed for the γ scheme in Fig. 2, the $-\frac{1}{2}$, $-\frac{3}{2}$ as well as the $\frac{1}{2}$, $\frac{3}{2}$ Zeeman levels of the Γ_8 ground state are degenerate for $H\|c$ correct to the order $\lambda'/10Dq$ in the g factors. Actually we have inferred a ≈ 1 cm^{-1} Γ_8 ground-state splitting from the g-factor analysis. Nevertheless, for the present purpose, this Γ_8 state mimics a cubic behavior since the zero-field splitting vanishes within the linewidth. The g factor of the excited Γ_8 level is zero in first order. Thus, for all accessible field strengths the solid transitions contribute to a single positive ZPL and their time-conjugated transitions give a single negative ZPL lower in energy by the ground-state Zeeman splitting. In other words, the γ_1 line at 1.4 K is expected to evolve into a simple derivative structure as is indeed observed in the 6-K spectrum. However, the appearance of the positive γ_2 line 4.6 cm^{-1} below the γ_1 zero position in the 6-K spectrum cannot be understood in the frame of static crystal-field theory. This also applies to the 25-K spectrum where the negative γ_2 peak occurs at exactly the position of the γ_1 1.4-K peak, thus indicating a sign reversal of the ground-state g factor. We believe one encounters manifestations of strong Jahn-Teller coupling of the $\Gamma_8{}^2E$ electronic state to an E-type vibrational mode. In such a case a vibronic spin doublet (tunneling singlet) approaches the Γ_8 vibronic ground state[12] which may account for the γ_2 peak at 6 K. Possibly the sign reversal occurring during the warm up from 1.4 to 25 K is a manifestation for the transition from a static to a dynamic Jahn-Teller effect. The comparatively very strong decrease of the γ_1 MCD intensity at 6 K most probably results from the larger linewidth for the γ site. Here, destructive interference effects between neighboring σ_+ and σ_- transitions are much more pronounced than for the sharper lines of the β and the α sites. For the *increased* γ-site MCD intensity at 25 K we suggest a similar effect.

TABLE III. Comparison of calculated and measured relative MCD intensities at 1.4 K; $u(\gamma)=0.85$), $u(\beta)=0.85$, $u(\alpha)=0.08$.

MCD line	Transition	MCD RTP	Relative MCD intensity calculated	Relative MCD intensity measured[b]
γ_1	$\sigma_+ -\frac{3}{2}\rightarrow -\frac{1}{2}$ $\sigma_- -\frac{3}{2}\rightarrow \frac{1}{2}$	$-\frac{1}{2}+\frac{9}{8}u$	+0.20[a]	+0.13
	$\sigma_+ -\frac{1}{2}\rightarrow \frac{1}{2}$	$\frac{1}{4}u$		
	$\sigma_- -\frac{1}{2}\rightarrow -\frac{3}{2}$ $\sigma_- -\frac{1}{2}\rightarrow \frac{3}{2}$	$-\frac{1}{2}+\frac{3}{8}u$		
β_1	$\sigma_+ -\frac{1}{2}\rightarrow \frac{1}{2}$	$\frac{1}{4}u$	+0.38[a]	+0.17
	$\sigma_+ -\frac{3}{2}\rightarrow -\frac{1}{2}$ $\sigma_- -\frac{3}{2}\rightarrow \frac{1}{2}$	$-\frac{1}{2}+\frac{9}{8}u$		
β_2	$\sigma_+ -\frac{1}{2}\rightarrow \frac{1}{2}$	$\frac{1}{8}u$	+0.15[a]	+0.11
	$\sigma_+ -\frac{3}{2}\rightarrow -\frac{1}{2}$ $\sigma_- -\frac{3}{2}\rightarrow \frac{1}{2}$	$\frac{1}{8}u$		
β_3	$\sigma_- -\frac{1}{2}\rightarrow -\frac{3}{2}$ $\sigma_- -\frac{1}{2}\rightarrow \frac{3}{2}$	$-\frac{1}{2}+\frac{3}{8}u$	−0.19	−0.19
α_3	$\sigma_- -\frac{1}{2}\rightarrow -\frac{3}{2}$ $\sigma_- -\frac{1}{2}\rightarrow \frac{3}{2}$	$-\frac{1}{2}+\frac{3}{8}u$	−0.47	−0.47
α_4	$\sigma_+ -\frac{1}{2}\rightarrow \frac{1}{2}$	$\frac{1}{4}u$	+0.02	−0.04

[a]Includes nonunity Boltzmann factor.
[b]Normalized to α_3.

We believe that the linewidths of the neighboring σ_+ and σ_- transitions become reduced because of motional effects in the ground state, resulting in reduced destructive interference. This effect may overcompensate the expected reduction in MCD intensity resulting from the reduced spin polarization at 25 K.

V. SUMMARY

MCD absorption and MCD-ESR data for the neutral vanadium impurity, $V^{4+}(3d^1)$, on the α, β, and γ sites in 6H-SiC were reported and supplemented by linearly polarized absorption and luminescence spectra. From the linearly polarized spectra, crystal-field-level schemes in zero magnetic field and the intensity parameter u were inferred for V^{4+} on each site. With this information the MCD ZPL positions, signs, and relative intensities could be accounted for without an adjustable parameter. The analysis of the optical data clearly shows that the trigonal crystal-field component of the α site is large compared to those of the γ and β sites. Evidence for vibronic coupling in both the ^2E ground state and the $^2T_2$ excited state is found but a detailed analysis of Jahn-Teller effects was not performed.

The MCD-ESR technique, in the present case, is site selective and even can be made strain selective. The V^{4+} resonances associated with the β and the γ sites are virtually identical showing that conventional ESR cannot distinguish between these two sites. The g factors for all three sites are satisfactorily explained in the frame of crystal-field theory.

ACKNOWLEDGMENTS

We thank K. Sambeth for expert technical assistance, S. Leibenzeder and R. Stein from Siemens AG for supplying the sample, and F. Fuchs, K. Maier, and J. Schneider for useful discussions. One of us (H.D.M) would like to thank B. Clerjaud for the hospitality during his stay at Universitée P. et M. Curie, Paris, where the high-resolution Fourier-transform absorption measurements were performed.

[1]G. Pensl and R. Helbig, in *Festkörperprobleme (Advances in Solid State Physics 30),* edited by U. Rössler (Vieweg, Braunschweig, 1990), p. 133.

[2]See, *Amorphous and Crystalline Silicon Carbide IV,* edited by C. Y. Yang, M. M. Rahman, and G. L. Harris, Springer Proceedings in Physics, Vol. 71 (Springer, New York, 1992).

[3]J. Schneider, H. D. Müller, K. Maier, W. Wilkening, F. Fuchs, A. Dörnen, S. Leibenzeder, and R. Stein, Appl. Phys. Lett. **56**, 1184 (1990).

[4]K. Maier, J. Schneider, W. Wilkening, S. Leibenzeder, and R. Stein, *Mater. Sci. Eng.* (1992), Vol. B11, p. 27; see also K. Maier, diploma thesis, University of Freiburg, 1991.

[5]K. Maier, H. D. Müller, and J. Schneider, Mater. Sci. Forum **83-87**, 1183 (1992).

[6]Th. Stiasny, R. Helbig, and R. A. Stein, in *Amorphous and Crystalline Silicon Carbide IV* (Ref. 2), p. 210.

[7]J. Reinke, S. Greulich-Weber, and J.-M. Spaeth, Solid State Commun. **85**, 1017 (1993).

[8]G. F. Koster, J. O. Dimmock, R. G. Wheeler, and H. Statz, *Properties of the Thirty-Two Point Groups* (MIT Press, Cambridge, 1963). For the irreducible representations of the T_d and the C_{3v} double group we use the Γ notation from this reference. For the T_d simple group, Mullikan's notation is used.

[9]W. Ulrici, J. Kreissl, D. G. Hayes, L. Eaves, and K. Friedland, Mater. Sci. Forum **38-41**, 875 (1989).

[10]R. E. Dietz, H. Kamimura, M. D. Sturge, and A. Yariv, Phys. Rev. **132**, 216 (1963).

[11]F. S. Ham, Phys. Rev. **138**, A1727 (1965).

[12]F. S. Ham, Phys. Rev. **166**, 307 (1968).

[13]A. Dörnen, Y. Latushko, W. Suttrop, G. Pensl, S. Leibenzeder, and R. Stein, Mater. Sci. Forum **83-87**, 1213 (1992).

[14]L. A. Boatner, R. W. Reynolds, Y. Chen, and M. M. Abraham, Phys. Rev. B **16**, 86 (1977).

[15]J. Kreissl, W. Ulrici, and W. Gehlhoff, Phys. Status Solidi B **155**, 597 (1989).

[16]S. Rodriguez, P. Fisher, and F. Barra, Phys. Rev. B **5**, 2219 (1972).

[17]If, e.g., a left circularly polarized transition is defined by the matrix element $\langle m_j|x+iy|m_{j'}\rangle$, its time conjugated transition is defined by the matrix element $\langle -m_j|x-iy|-m_{j'}\rangle$.

[18]A. Bhattacharjee and S. Rodriguez, Phys. Rev. B **6**, 3836 (1972).